AUT Journal of Civil Engineering

AUT J. Civil Eng., 5(3) (2021) 403-420
DOI: 10.22060/ajce.2021.19213.5721

Estimating the Sand Shear Strength from Its Grain Characteristics Using an Artificial Neural Network Model and Multiple Regression Analysis

M. Mousavi, M. Jiryaei Sharahi*

Civil Engineering Department, Qom University of Technology, Iran.

ABSTRACT: Determination of soil shear strength is always among the most important issues in geotechnical problems. In this research, various neural network models and multiple regression are developed to obtain shear strength parameter of the sandy soil from physical parameters of roundness (R), maximum and minimum dry densities (γdmax, γdmin), relative density (Dr), and grain sizes, D10, D30, D50, and D60. Firstly, the effect of these physical parameters on the shear strength of sands is examined by soil laboratory tests. For this purpose, laboratory tests of the direct shear, maximum and minimum dry densities, and sieve analysis are conducted. Subsequently, the laboratory results are used as a data set to develop an artificial neural network and multiple regression models to predict shear strength parameters. Finally, the efficiency and appropriateness of each approach are discussed. Results showed that both neural network and regression are precise, appropriate, and inexpensive methods to predict soil shear strength parameters.

Review History:

Received: Nov. 04, 2020
Revised: Oct. 28, 2021
Accepted: Nov. 24, 2021
Available Online: Dec. 04, 2021

Keywords:

Neural network
Multiple regression
Sand
Shear strength
Grain characteristics

1- Introduction

Determination of soil shear strength is essential in geotechnical problems such as foundation design, retaining walls, and slope stability. To determine geotechnical parameters of soil laboratory and in-situ tests are used, which are time and cost-consuming. Prediction methods such as artificial neural networks and multiple regression as inexpensive methods can be applied to predict geotechnical parameters of soil. Before implementing these methods, recognition of the influence of various physical properties on the shear strength of sand is necessary.

Previous studies indicate that the shear strength of soil depends on various parameters such as grain size distribution, relative density, particle shape. Researches show that the friction angle of shearing resistance increases as the constituent particle sizes increase [1-7]. Wang et al. (2013) performed a series of direct shear box tests and triaxial tests to characterize the shear strength of the accumulation soil. Results show that the angle of shearing resistance generally increases with increasing median particle diameter and gravel content and decreases with the increasing coefficient of uniformity [7]. However, other researchers found different results [8-11]. Their results indicate that the angle of shearing resistance reduces with the increase of particle size. Meanwhile, Vangla et al. (2015) resulted that the particle size does not affect the peak friction angle [12]. Koerner et al. (1970) indicated that there is an increase in strength with decreasing effective size, particularly with sizes less than 0.06 mm. Also, at a given relative density, the influence of different soil gradations has little effect on soil strength [13]. Therefore to clarify the ambiguities in the literature results, further investigation needs to be conducted. Shang et al. (2020) concluded that a large cohesion, defined as the interlocking cohesion, appears in gravels and increases as the average particle size and relative density increase [14]. Alias et al. (2014) concluded that the effective internal friction angle could depend on particle size, and tests with larger particles produce a higher effective internal friction angle and develop high shear strength [15]. Zhang et al. (2019) also concluded that the deformation declines with the decrease in particle size [16]. Boudia et al. (2021) show that the particle size and distribution directly affect the mechanical behavior of the dune sand, and the dominant size class governs the natural sand behavior [17]. Various studies show that the soil strength increases with increasing angularity or decreasing roundness [2, 13, 18-19]. Zelasko et al. (1975) concluded that particle roundness and relative density significantly influence the shear strength. Particle shape can be described by roundness, sphericity, and surface texture [11]. Sphericity in general falls in a narrow range for natural sands [20-21], and surface texture is a second-order feature and highly variable that is difficult to measure [18]. Hence only roundness can be used

*Corresponding author's email: jiryaei@qut.ac.ir

readily to characterize particle shape [19].

Many researchers have attempted to implement artificial neural networks (ANNs) to model geomaterials' constitutive behavior. Juang et al. (2002) developed a system of neural networks for predicting D_r, K_0, and OCR of sands from CPT measurements [22]. Ellis et al. (1995) applied artificial neural networks to model sands' stress-strain relationship with varying grain size distribution and stress history [23]. Ghaboussi and Sidarta (1998) developed nested adaptive neural networks for modeling the constitutive behavior of geomaterials [24]. Zhu et al. (1998) developed a Recurrent Neural Network (RNN) to model the residual soil's shear behavior. They show that the RNN model can simulate shearing behavior, softening and hardening characteristics of the soil, isotropic and anisotropic consolidation conditions, and pore water pressure in undrained conditions [25]. However, the artificial neural network has not been implemented to predict friction angle from grain physical properties.

Regression is a statistical process that can be used to estimate relationships among dependent geotechnical parameters. Bareither et al. (2008) developed a multiple regression model based on effective particle size, maximum dry unit weight, and roundness to predict the friction angle of compacted sands [19]. But the relationship provided for very dense sand, hence a general model can be developed using multiple regression techniques.

In this research, the effects of physical characteristics of grain size distribution, relative density, particle size, and roundness on the friction angle of sand are examined. For this purpose, laboratory tests of direct shearing, relative density, and sieve analysis are employed. Roundness is determined using a visual procedure developed by Krumbein [26]. Subsequently, artificial neural networks and multiple regression methods are developed to estimate friction angle from characteristics of grain size distribution, relative density, particle size, and roundness. A proper backpropagation algorithm and appropriate transfer functions need to be selected to enhance the accuracy of the ANN model. For this purpose, several backpropagation algorithms and transfer functions are examined. Finally, the efficiency and accuracy of each approach are discussed.

2- Shear strength of the soils

For the soil mass to be stable when different loads are applied, it must have sufficient strength. Shear strength is the basis of calculations for solving many problems related to real structures such as the bearing capacity of foundations, slopes stability, stability of earth dams and retaining walls, earthquake resistance, and soil liquefaction. The Coulomb failure criterion is one of the key issues in understanding many engineering geology and geotechnics concepts. Based on the Coulomb failure criterion, the Shear strength is a combination of the frictional and the cohesion components:

$$\tau_f = c + \sigma \tan\phi \quad (1)$$

Where τ_f is the failure shear stress, σ represents the normal stress, and ϕ and c are the internal frictional angle and the cohesion, respectively.

3- Laboratory Testing Program

3- 1- Preparation of Samples

Three types of sandy soils were sampled around Qom (Iran) to conduct soil laboratory tests. Two types, type 1 and type 2, are well-graded, and the other, type 3, is uniform fine sand. Sieve analysis tests are carried out for each sample. Fig. 1 shows original sample particles passing through sieve #200 and remaining on sieve #4 (particle size between 4.75 to 0.075 mm). The original sample is divided into three fractions; fine (< 0.425 mm and > 0.075 mm), medium (< 2.0 mm and > 0.425 mm), and coarse (< 4.75 mm and > 2.0 mm). Particle size distribution curves for each sample and its three sandy fractions are shown in Figs. 2 to 4. Fig. 2 shows the particle size distribution curve for sand 1, including the original, fine, medium, and coarse fractions. Fig. 3 also shows these fractions for sand 2. Fig. 3 depicts the particle size distribution curve for sand 1. Parameters obtained from these curves are summarized in Table 1. Two Samples are classified as well-graded sand (SW); their fractions and 3rd sand are classified as poorly graded sand (SP) according to the Unified soil classification system in ASTM D2487 [27].

3- 2- Roundness (R)

Based on Krumbein's chart [26], Edil et al. (1975) reported that viewing at least 25 particles yield a reliable mean roundness [21]. Thirty particles of each sample are used to obtain the roundness (R) based on Krumbein's chart [21], as shown in Table 2. Table 2 shows the roundness categories, including angular, subangular, subrounded, rounded, and well rounded, and also, the range of the roundness and the average are proposed for any category. Fig. 5 shows an image of the particle shapes in sand 1. This image shows that an average roundness can be considered because various particle shapes are observed. Observed values of roundness are summarized in Table 3. The roundnesses for sand 1 and 2 are 0.34 and for sand three is 0.66. It means that sandy samples of 1, 2, and 3 are classified as rounded, rounded, and subangular, respectively.

3- 3- Minimum and maximum dry density tests

The maximum dry density (γ_{dmax}) and minimum dry density (γ_{dmin}) tests on samples are conducted based on ASTM D4253 [28], and ASTM D4254 [29]. Using values for maximum and minimum dry densities and current dry density (γ_d), relative density (D_r) can be determined by the following equation.

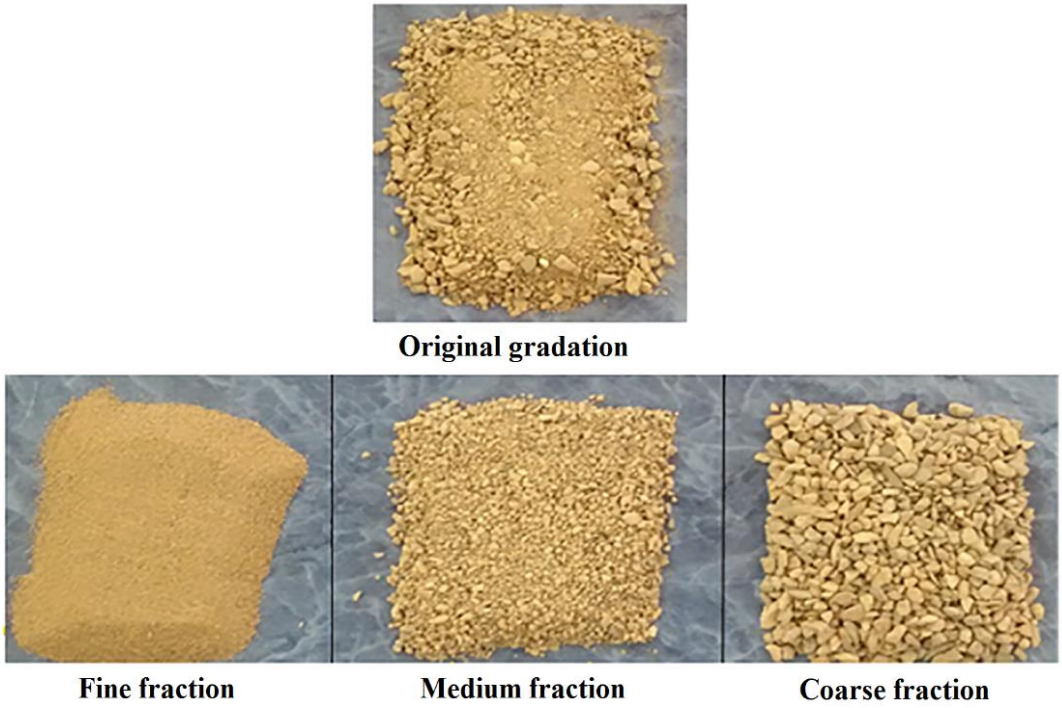

Fig. 1. Image of original and fractions of sand 1.

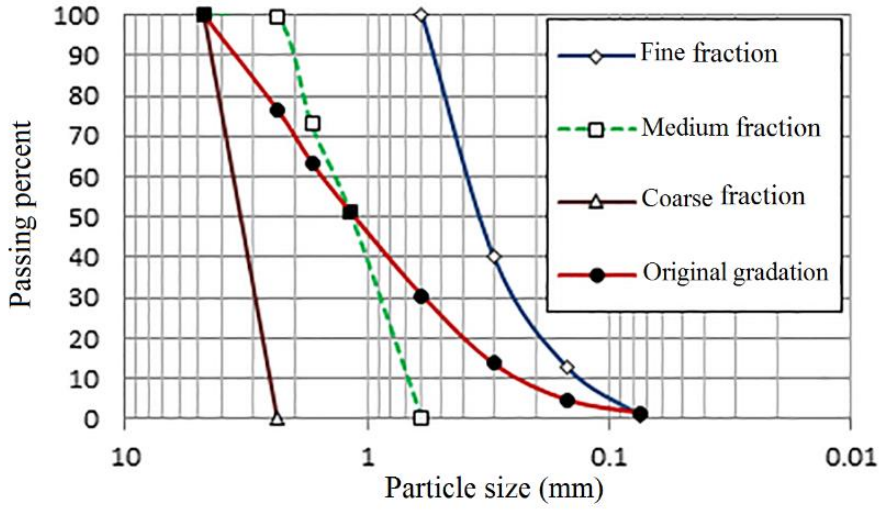

Fig. 2. Grain size distribution curves of sand 1.

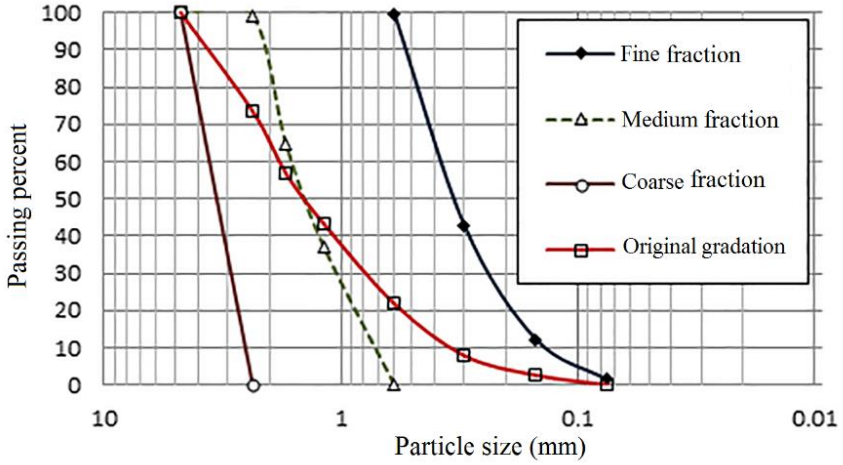

Fig. 3. Grain size distribution curves of sand type 2.

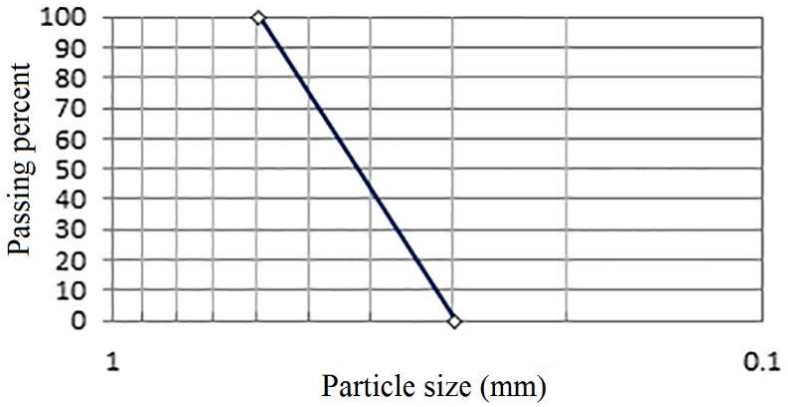

Fig. 4. Grain size distribution curves of sand 3.

Table 1. Grain size distribution characteristics for each sample.

Sand type	Gradation	D10	D30	D50	D60	CU	CC	Classification (ASTMD2487)
1	Original gradation	0.22	0.59	1.01	1.4	6.36	1.13	SW
1	Fine fraction	0.13	0.25	0.35	0.4	3.08	1.2	SP
1	Medium fraction	0.7	0.9	1.05	1.2	1.71	0.96	SP
1	Coarse fraction	2.3	3	3.2	3.7	1.61	1.06	SP
2	Original gradation	0.31	0.8	1.3	1.9	6.10	1.37	SW
2	Fine fraction	0.14	0.24	0.33	0.38	2.71	1.08	SP
2	Medium fraction	0.72	1.05	1.42	1.61	2.24	0.95	SP
2	Coarse fraction	2.54	2.92	3.35	3.60	1.42	0.93	SP
3	Fine sand	0.32	0.37	0.42	0.45	1.40	0.95	SP

Fig. 5. Image of particle shape for sand 2.

Table 2. Roundness categories for Krumbein images (Edil et al., 1975).

Roundness	Krumbein Image	Range	Average
Angular	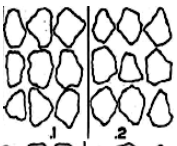	0.10-0.26	0.18
Subangular	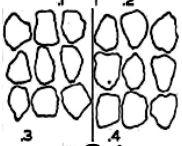	0.26-0.42	0.34
Subrounded		0.42-0.58	0.5
Rounded	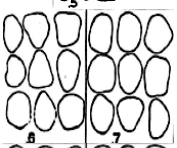	0.58-0.74	0.66
Well-rounded	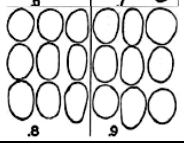	0.74-0.90	0.82

Table 3. Roundness (R) values obtained for samples.

Sand type	Original gradation	Fine fraction	Medium fraction	Coarse fraction
1	0.34	0.42	0.42	0.26
2	0.34	0.26	0.26	0.42
3	0.66	---	---	---

Table 4. minimum and maximum dry densities.

Sand type	Original gradation		Fine fraction		Medium fraction		Coarse fraction	
	γ_{dmin}	γ_{dmax}	γ_{dmin}	γ_{dmax}	γ_{dmin}	γ_{dmax}	γ_{dmin}	γ_{dmax}
1	1.40	1.87	1.30	1.68	1.34	1.68	1.34	1.6
2	1.61	1.99	1.4	1.69	1.44	1.72	1.45	1.76
3	1.35	1.65	---	---	---	---	---	---

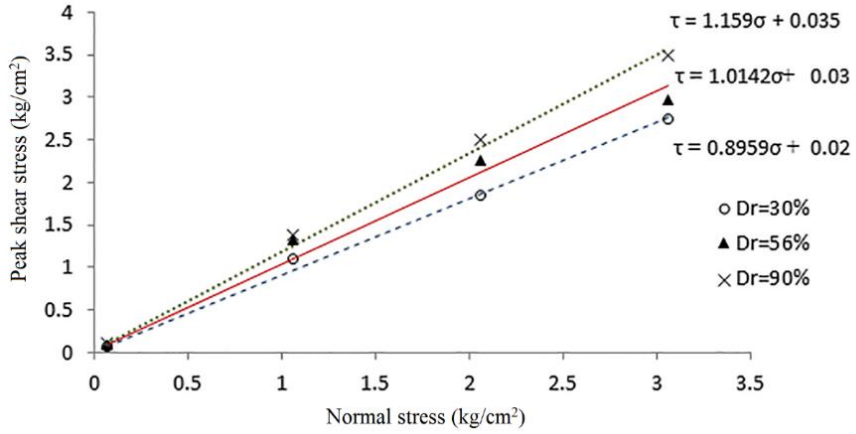

Fig. 6. Coulomb failure envelopes as a linear curve-fitting for sand 2.

$$D_r = \frac{\gamma_d - \gamma_{d\min}}{\gamma_{d\max} - \gamma_{d\min}} \times \frac{\gamma_{d\max}}{\gamma_d} \quad (2)$$

Obtained values for maximum and minimum dry densities and relative density are listed in Table 4. Variation in minimum and maximum dry densities of sand 3, and all fractions of sand 1&2 which are classified as poorly graded sand, is not significant. A greater amount of maximum dry density is obtained for the original gradation of sands 1&2 which are well graded.

3- 4- Direct shear tests

To determine the internal friction angle of sands and their fractions direct shear tests are carried out in a 100-mm-wide square shear box, following the procedure in ASTM D3080 [30]. Direct shear tests are carried out on 108 dry samples of sand with three various relative densities under normal stresses approximately equal to 0.06, 1, 2, and 3 kg/cm^2. In shear strength tests on sandy soil, a little cohesion usually appears that depends on the relative density of the sample, particles size, and friction in the shear box. The direct shear test with the normal stress of 0.06 kg/cm^2 is considered to obtain such cohesion exactly.

Failure is defined as the shear stress corresponding to the initial horizontal tangent to the shear stress-displacement curve. For samples exhibiting a peak point in the shear stress-displacement curve, failure is defined at peak shear stress. Coulomb failure envelopes are determined by linear least-squares curve-fitting that passes through four points, as shown in Fig. 6. Coulomb failure envelopes correspond to three relative densities of 30 %, 56 %, and 90 % of sand 1.

Table 5. Peak friction angle for sand 1 and its fractions.

Dr	Original gradation	Fine fraction	Medium fraction	Coarse fraction
35	39.2	36.6	40.9	43.2
60	43.9	37.4	42.8	46.3
85	45.8	38.1	45.6	47.7

Table 6. Peak friction angle for sand 2 and its fractions.

Dr	Original gradation	Fine fraction	Medium fraction	Coarse fraction
30	41.9	37.3	39.0	44.9
56	45.4	39.4	44.0	47.8
90	49.2	40.9	48.4	51.3

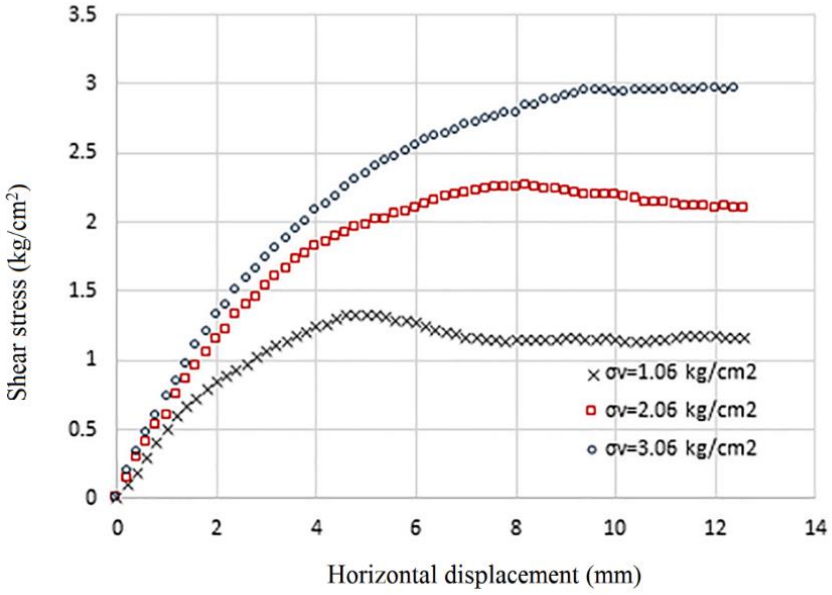

Fig. 7. Shear stress-displacement curves for sand 2 with the relative density of 56 percent.

4- Laboratory test results

The peak friction angle of 27 samples of sands and their fractions with various relative densities are summarized in Tables 5 to 7. Table 5 lists the friction angles for the original gradation and also various fractions of sand 1. The friction angle of original gradation is lower than that of the coarse fraction, greater than that of the fine fraction, and approximately equal to that of the medium fraction. Table 6 shows the friction angles for the original gradation and also various fractions of sand 2. Table 7 shows the friction angle values for different relative densities of the sand 3.

Fig. 7 shows shear stress-displacement curves corresponding to sand 2 with normal stresses of 1.06, 2.06, and 3.06 kg/cm^2. The peak point is more obvious in the curve corresponding to the normal stress of 1.06 kg/cm^2 than other curves with greater normal stresses. Hence, a peak appears in the curve for lower normal stress than a limit normal stress (σ_l) that in this study is equal to 2.06 kg/cm^2. In granular materials, especially in dense states, shearing

Table 7. Peak friction angle for sand 3..

Dr	Sand type 3
30	34.3
78	36.6
90	36.7

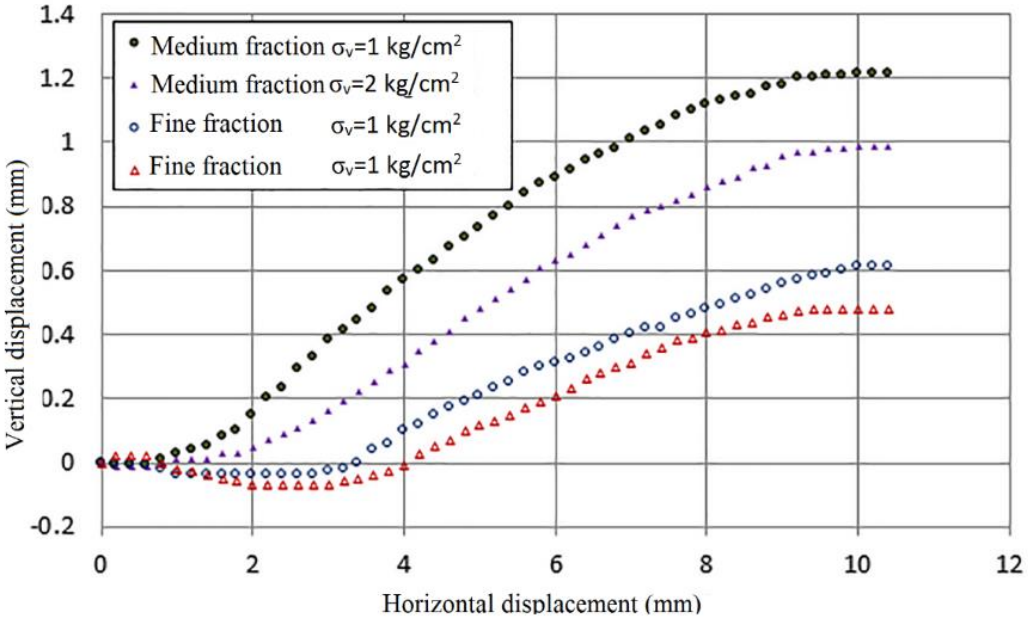

Fig. 8. Vertical displacement due to dilation vs. horizontal displacement for fine and medium fractions of sand 2 in relative density of 56 %.

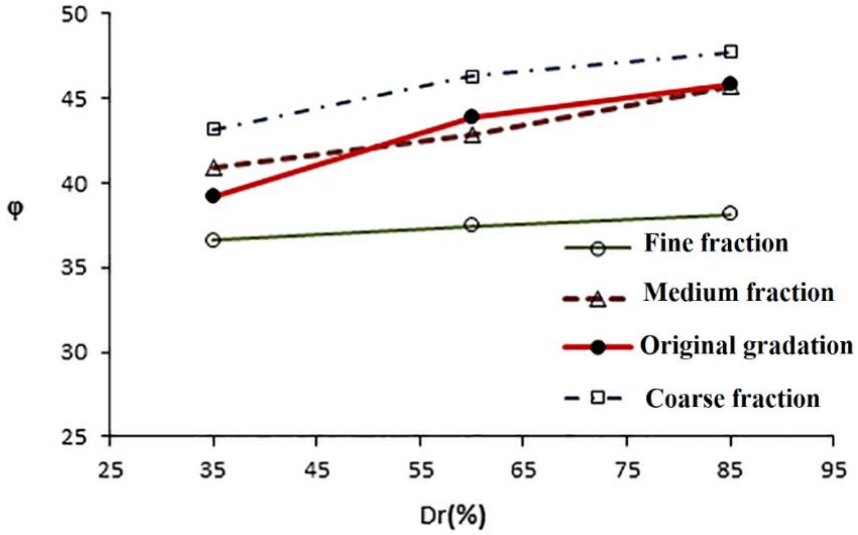

Fig. 9. Friction angle vs. relative density for sand 1 and its fractions..

is associated with dilation due to grains interlocking with each other. With increasing dilation, the peak point appears in the shear stress-displacement curve. Fig. 8 shows vertical displacement due to dilation for fine and medium fractions of sand 2. As depicted in Fig. 8, vertical displacement due to dilation increases with reducing normal stress. Additionally, more vertical displacement or dilation occurs in samples with larger particle sizes.

Fig. 9 shows that the relative density has a significant effect on the friction angle. Moreover, with constant relative density, friction angle increases with particles size. Notable that the friction angle of the original gradation of each sand is approximately equal to that of the medium fraction.

Friction angle as a function of effective diameter (D_{10}) for sand 1 with various relative densities is shown in Fig. 10. As can be seen, with constant relative density friction angle

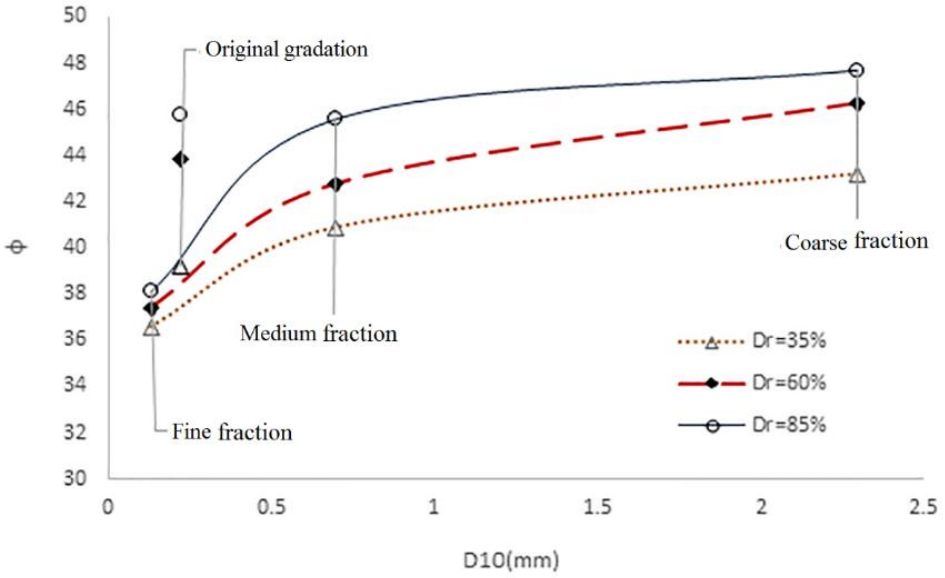

Fig. 10. Friction angle as a function of D10 for sand type 1 and its fractions.

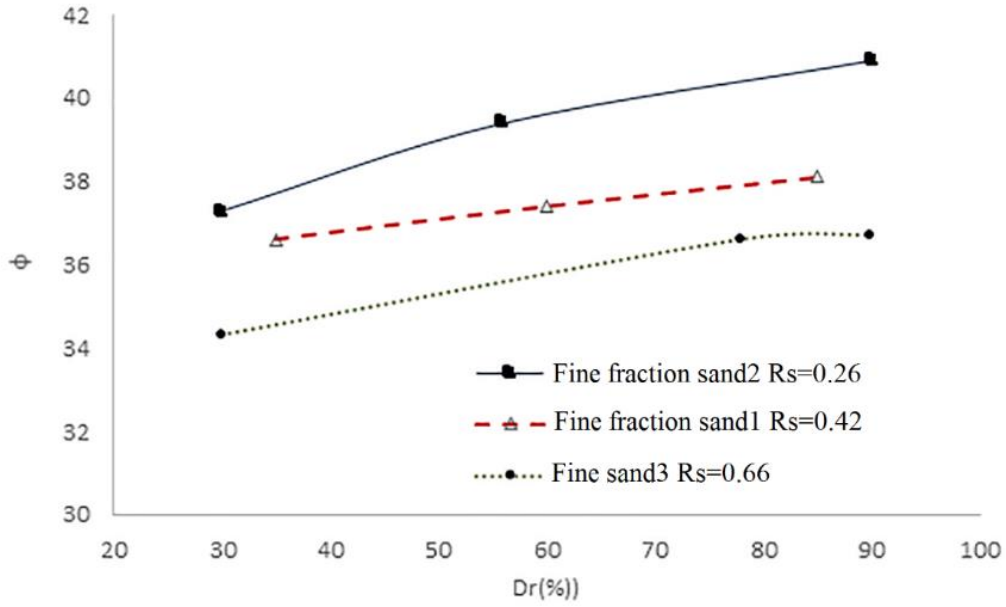

Fig. 11. Friction angle as a function of roundness and relative density.

increases with D_{10}, and D_{10} is more effective to enhance friction angle in original gradation as well-graded sand than its fractions as poorly graded sands. Similar results can be deduced for D_{30}, D_{50}, and D_{60}. In general, with constant relative density friction angle increases with constituent particles size. From Fig. 10, the rate of increase in friction angle for diameters from 0.1 to 0.7 mm is greater than that for the larger diameters. In other words in fine sands, increasing particle size enhances shear resistance more significantly than in medium or coarse sands.

Fig. 11 shows friction angle as a function of relative density and roundness for samples of fine sands. As expected, an increase in roundness leads to a reduction in friction angle.

5- Artificial Neural Network

Artificial Neural Network (ANN) consists of interconnected processing elements or neurons that are arranged in several layers, including the input layer, hidden

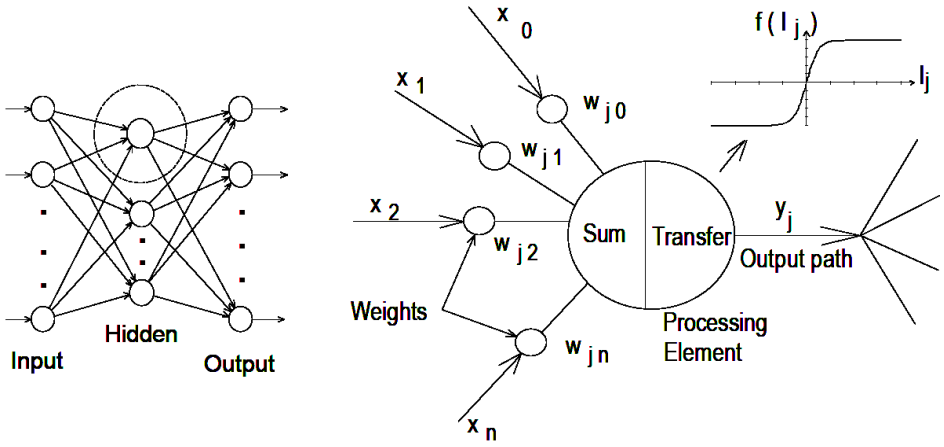

Fig. 12. Components of neural network.

layers, and output layer. Fig. 12 shows the components of an artificial neural network.

The neural network can train complex relations between variables to predict unknowns. The output from each neuron in the previous layer (i) provides the input for the next layer (j). At k^{th} neuron in the j^{th} layer, inputs from neurons in previous layers (X^i_k) are multiplied by adjustable weights (w_{ik}). Weighted inputs are summed and added to a threshold value (θj).

$$n_k^j = \sum_{k=1}^{K} w_{ik} X_k^i + \theta_j \tag{3}$$

The transfer function is also an essential element in neural networks. There are different types of transfer functions that are implemented according to the nature of the problem. Transfer function $f(n^j_k)$ is used to estimate outputs of neurons in layer j as:

$$y_k^j = f\left(n_k^j\right) \tag{4}$$

Estimated output (ŷ) is compared with the target value (y), and if the difference is greater than the specified, weights will be modified. Every step of correcting the weight is named an epoch, and this weight modification process is a backpropagation error. In this study, the multilayer perceptron neural network (MLP) is used in which the input layer consists of independent components. MLP network with a hidden layer and an output layer can be used for the estimation of nonlinear relationships. Therefore, a hidden layer and an output layer are assumed for the neural network architecture.

The input layer contains neurons of D_{10}, D_{30}, D_{50}, and D_{60} representing grain size distribution, γ_{dmax}, γ_{dmin} representing constituent minerals of particles, R representing particle shape, and D_r representing relative density, and the output layer contains friction angle. A total number of 27 data are used in this study that 21 of them were assigned to network training, and 6 of them are assigned to network testing. The data that has been underlined in Tables 5 to 7 are assigned for testing and other data are assigned for the training phase of the neural network. To identify appropriate algorithms for processing of backpropagation, several training algorithms, including Resilient Propagation (RPROP) [31], Marquardt – Levenberg (ML) [32], Bayesian (B) [33-34], Scaled Conjugate Gradient (SGC) [35] are examined. In addition, to determine proper transfer function for neural network, available transfer functions such as hyperbolic tangent sigmoid (tansig), logistic sigmoid (logsig), linear (purelin), and radial basis (radbas) function are investigated.

Table 8 shows neural network models, training and testing with the various number of neurons in the hidden layer and considering various backpropagation algorithms. R-value is the root of R-squared that can be obtained as:

$$R^2 = 1 - \frac{\sum_{i=1}^{n}\left(\hat{y}_i - y_i\right)^2}{\sum_{i=1}^{n}\left(y_i - \bar{y}_i\right)^2} \tag{5}$$

In which $\hat{y}_i$ is the estimated output and $\bar{y}$ is the mean of the target (y_i). From Table 8, model prediction ability is outstanding because R-value in the training and test phases are close to 1. Results show that influences of kind of backpropagation algorithm and number of neurons in the hidden layer are not significant. In addition, the accuracy

Table 8. Neural Network Models.

Model No	Backpropagation algorithm	Number of neurons in the hidden layer	Transfer function in the hidden layer	Transfer function in the output layer	*R*-value train	*R*-value test
1	RPROP	4	tansig	purelin	0.997	**0.941**
2	RPROP	8	tansig	purelin	0.998	**0.975**
3	RPROP	16	tansig	purelin	0.998	**0.964**
4	B	4	tansig	purelin	0.968	**0.941**
5	B	8	tansig	purelin	0.968	**0.941**
6	B	16	tansig	purelin	0.946	**0.925**
7	ML	4	tansig	purelin	0.998	**0.952**
8	ML	8	tansig	purelin	0.998	**0.962**
9	ML	16	tansig	purelin	0.998	**0.952**
10	SCG	4	tansig	purelin	0.998	**0.972**
11	SCG	8	tansig	purelin	0.998	**0.974**
12	SCG	16	tansig	purelin	0.998	**0.973**
13	RPROP	8	logsig	purelin	0.998	**0.958**
14	RPROP	8	radbas	purelin	0.998	**0.821**

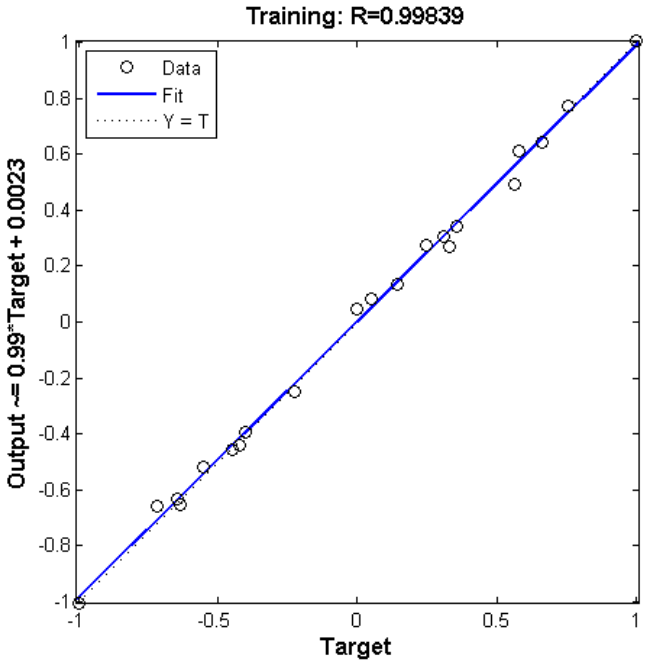

Fig. 13. Training performance (R-value) of neural network model No.2.

of network models combining hyperbolic tangent sigmoid function in the hidden layer and linear transfer function in the output layer is acceptable. However, prediction of the network model with radial basis transfer function in the hidden layer IS less accurate in the testing phase than hyperbolic tangent sigmoid function or logistic sigmoid transfer function.

As shown in Fig. 13, neural network (mode 2) with hyperbolic tangent sigmoid function in the hidden layer and linear function in the output layer is trained with excellent R-value (0.998), and scattering values of the target around predicting model is very low. In Fig. 14, the regression of the testing phase for laboratory-measured values and predicted friction angle by the network can be observed. The R-value of 0.975 indicates that the network prediction is accurate in the testing phase. Network performance for the training phase is shown in Fig. 15. It is observed that training mean

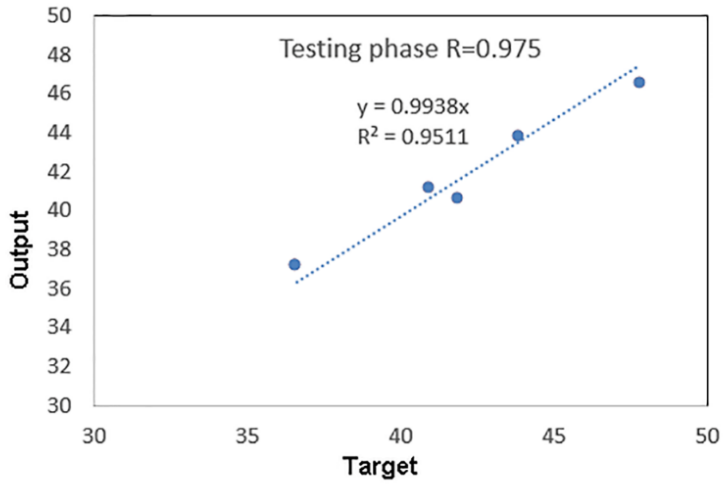

Fig. 14. Testing performance (R-value) of neural network model 2.

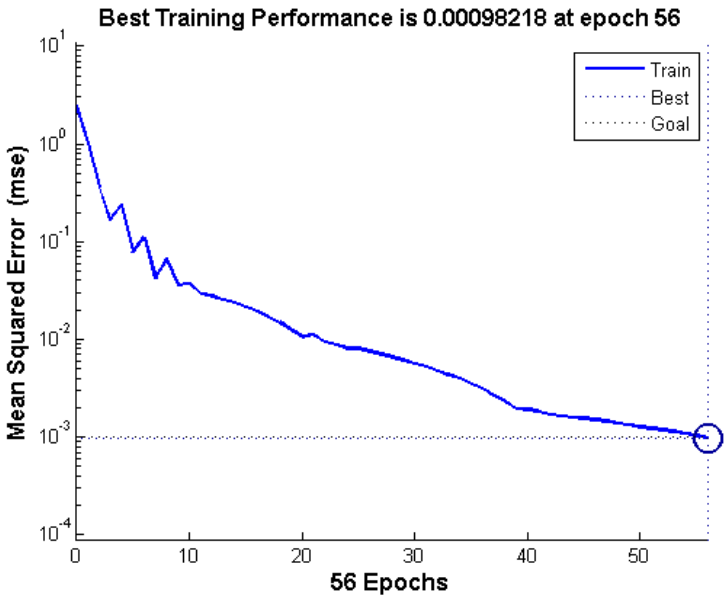

Fig. 15. Epochs in the training phase of neural network model 2.

squared error is approached to a purposed error of 0.001 in a few epochs (56 epochs). Therefore network model quickly approaches the target value. Fig. 16 shows the capability of the neural network model in forecasting values of friction angle that were never experienced in the training phase.

6- Multiple regression

Multiple regression attempts to predict unknown variables as a response or target from several variables as predictors by fitting a mathematical function to observed data. Multiple regression is employed to fitting a function of physical parameters including roundness (R); maximum and minimum dry densities (γ_{dmax}, γ_{dmin}); relative density ($D_{r)}$, and grain sizes; D_{10}, D_{30}, D_{50}, and D_{60} to obtain shear strength parameter; the friction angle for sands in dry condition. Regression can be conducted in two manners: linear and nonlinear regression. Although the nature of the problem is nonlinear linear regression is a simple statistical model and easily applicable for solving problems. Hence, at first, a linear regression assumed to obtain friction angle as:

$$\varphi = \alpha_1 + \alpha_2 D_{10} + \alpha_3 D_{30} + \alpha_4 D_{50} + \alpha_5 D_{60} + \alpha_6 R + \alpha_7 \gamma_{dmax} + \alpha_8 \gamma_{dmin} + \alpha_9 D_r \quad (6)$$

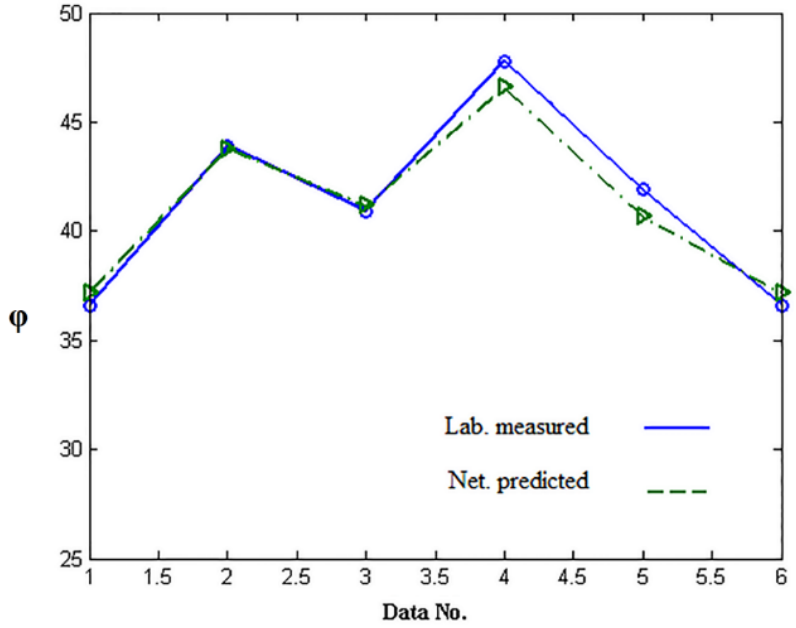

Fig. 16. Comparing friction angle measured in the laboratory and predicted by the network model 2.

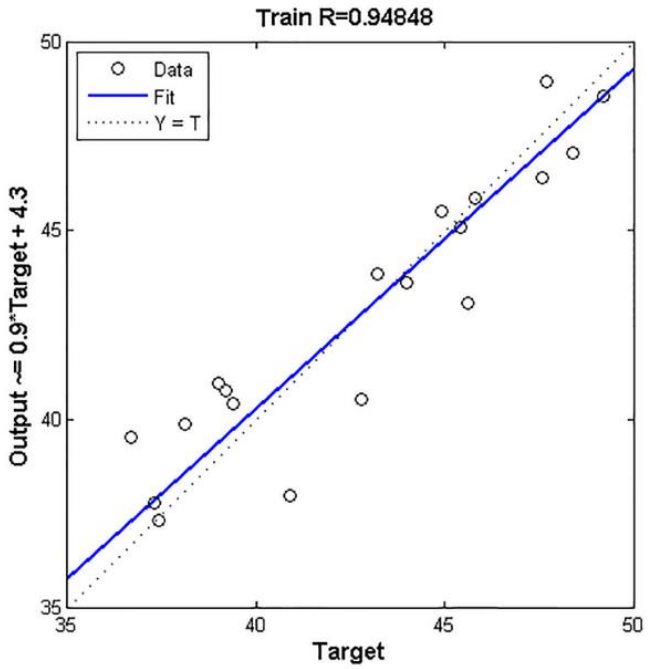

Fig. 17. Training performance (R-value) in linear regression.

Linear least square curve fitting is performed with QR decomposition algorithm [36] to obtain coefficients of α_i as:

$$\varphi = \begin{bmatrix} 22.305 + 16.201D_{10} - 19.795D_{30} - 7.808D_{50} + 14.524D_{60} \\ -11.129R - 2.840\gamma_{dmax} + 14.036\gamma_{dmin} + 0.102D_r \end{bmatrix} \quad (7)$$

Fig. 17 shows R-value in the training phase. R-value of 0.948 reveals that the training phase has been done well. Also, the R-value of 0.93 in Fig. 18 shows the ability of the model to predict the friction angle. Friction angles from Eq. (6) in comparison with those measured in the laboratory are depicted in Fig. 19. Obtained values in linear regression are not very accurate; however, approximation of linear

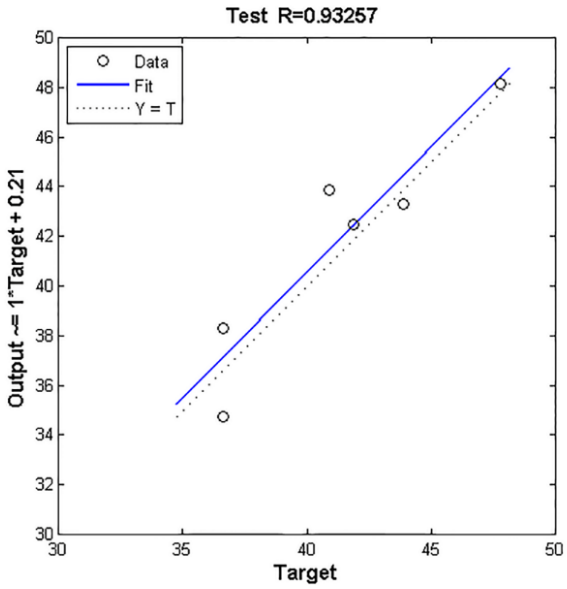

Fig. 18. Testing performance (R-value) phase for linear regression.

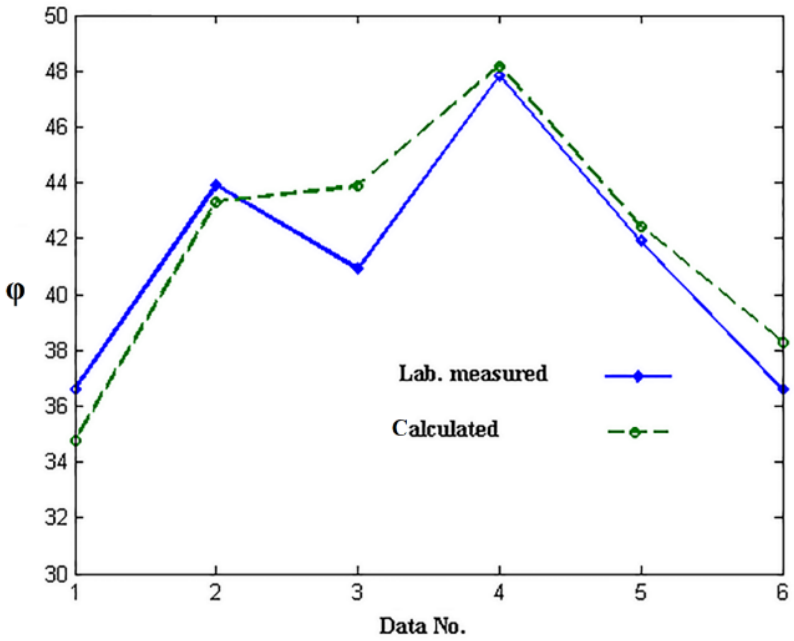

Fig. 19. Comparing friction angle measured in the laboratory and predicted by the linear regression.

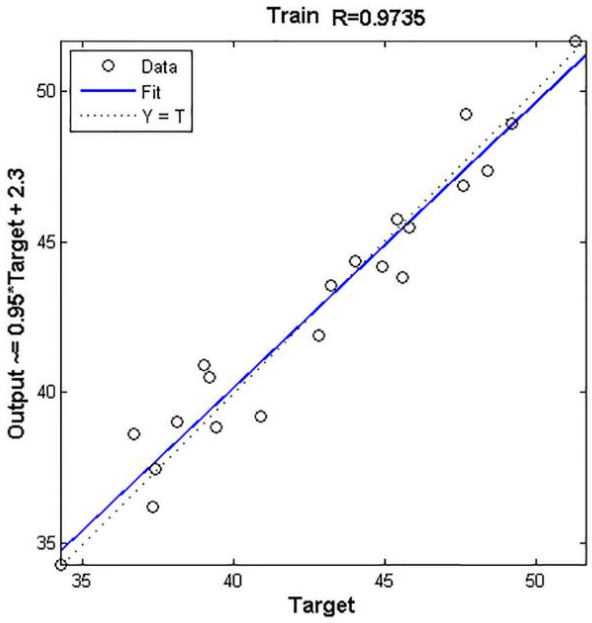

Fig. 20. Performance (R-value) of training phase in nonlinear regression.

regression is valuable because of the simplicity of the corresponding formula.

Since soils behavior is nonlinear, the calculation of nonlinear regression is expected to be more accurate. To carry out nonlinear regression following function is assumed:

$$\varphi = \beta_1 + \frac{\gamma_{dmax}^{\beta_3} D_r^{\beta_5}}{R^{\beta_2} \gamma_{dmin}^{\beta_4}} \left(\beta_6 D_{10}^{\beta_7} + \beta_8 D_{30}^{\beta_9} + \beta_{10} D_{50}^{\beta_{11}} + \beta_{12} D_{60}^{\beta_{13}} \right) \quad (8)$$

Marquardt – Levenberg nonlinear least square algorithm [37] is used for curve fitting Eq. (7) to observed data and determine coefficients of β_i.

$$\varphi = 20.424 + \frac{\gamma_{dmax}^{2.098_3} D_r^{0.248}}{R^{0.233} \gamma_{dmin}^{0.509}} \times \left(1.871 D_{10}^{0.239} + 0.662 D_{30}^{-0.0016} + \right. \quad (9)$$

$$\left. 0.058 D_{50}^{-0.191} + 0.044 D_{60}^{-0.165} \right)$$

Fig. 20 shows R-value for the training phase in nonlinear regression. The R-value of training phases is 0.974. Fig. 21 shows R-value for the test phase in nonlinear regression is 0.979. These R-values reveal that the performance of nonlinear regression is more accurate in comparison with linear regression. The scattering of values of targets around fitted function is lower than linear regression but is higher than the neural network model (Figs. 13 and 14). Fig. 22 shows a comparison of calculated friction angles by Eq. (8) with that measured in the laboratory. An advantage of regression is the simplicity of mathematical formula that can be improved.

7- Conclusion

In this research, the effects of physical characteristics of grain size distribution, relative density, particle size, and roundness on the friction angle of sand were examined. For this purpose, laboratory tests of direct shearing, relative density, and sieve analysis were employed. Roundness was determined using a visual procedure developed by Krumbein. From these laboratory tests, it is concluded that:

(i) With increasing dilation, the peak point appears in the shear stress-displacement curve. The peak appears in the curve for lower normal stress than a limit normal stress (σ_l). Vertical displacement due to dilation increases with reducing normal stress. Additionally, more vertical displacement or dilation occurs in samples with larger particle sizes.

(ii) Relative density has a significant effect on the friction angle. With constant relative density, friction angle increases with particles sizes,

(iii) An increase in roundness reduces friction angle.

(iv) The rate of increase in friction angle for diameters from 0.1 to 0.7 mm is greater than that for the larger diameters.

In other words, increasing particle size enhances shear resistance more significantly in fine sands than in medium or coarse sands. Subsequently, artificial neural networks

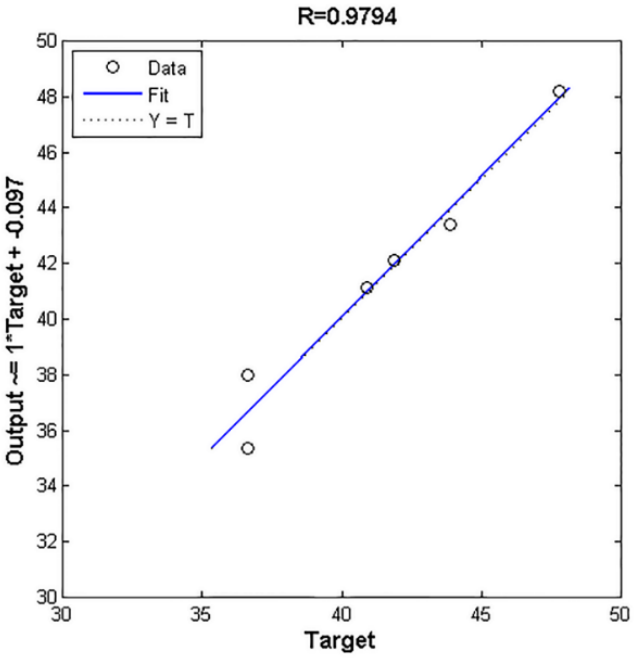

Fig. 21. Performance (R-value) of the testing phase in nonlinear regression.

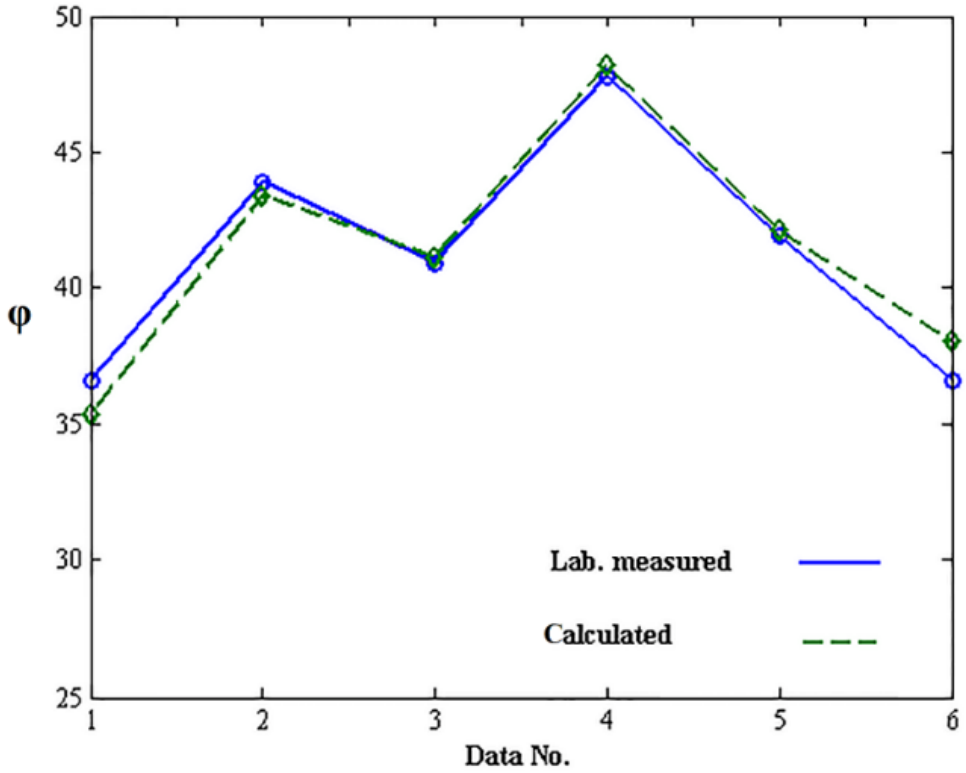

Fig. 22. Comparing friction angle measured in the laboratory with predicted by nonlinear regression.

and multiple regression methods were developed to predict friction angle from characteristics of grain size distribution, relative density, particle size, and roundness. In ANN models, several backpropagation algorithms, transfer functions, and the number of neurons were examined. Results show that the influences of the kind of backpropagation algorithm and the number of neurons in the hidden layer are not significant. Additionally, the accuracy of network models combining hyperbolic tangent sigmoid function in the hidden layer and linear transfer function in the output layer is acceptable. Obtained values in linear regression are not very accurate; however, approximation of linear regression is valuable due to the simplicity of the corresponding formula. The performance of nonlinear regression is more accurate in comparison with linear regression. An advantage of regression is the formula's simplicity which can be improved because its mathematical expression is explicit. However, the accuracy of regression is less than the accuracy of the artificial neuron network.

References

[1] J. Kolbuszewski, M.R. Frederick, The significance of particle shape and size on the mechanical behavior of granular materials, European Conference on Soil Mechanics and Foundation Engineering (Wiesbaden) Sec.4 Paper 9, 1963.

[2] E. Zolkov, G. Wiseman, Engineering Properties of Dune and Beach Sands and the Influence of Stress History, Proc. of Sixth Int. Conf. on SMFE, vol. I, 1965.

[3] J.A. Charles, K.S. Watts, The influence of confining pressure on the shear strength of compacted rockfill, Géotechnique, 30(4) (1980) 353-367.

[4] T. Nakao, S. Fityus, Direct shear testing of a marginal material using a large shear box, Geotechnical Testing Journal, 31(5) (2008) 1-11.

[5] M.N. Islam, A. Siddika, M.B. Hossain, A. Rahman, M.A. Asad, Effect of Particle Size on the Shear Strength Behavior of Granular Materials, Journal of Australian Geomechanics, 46 (3) (2011) 75-86.

[6] E.M. Kara, M. Meghachou, N. Aboubekr, Contribuion of particle size ranges to sand fraction, ETASR- Engineering Technology & Applied Science Research, 3(4) (2013) 497-501.

[7] J. Wang, H.-P. Zhang, S.-C. Tang, Y. Liang, Effects of Particle Size Distribution on Shear Strength of Accumulation Soil, Journal of Geotechnical and Geoenvironmental Engineering, 139(11) (2013) 1994-1997.

[8] W.M. Kirkpatric, Effects of Grain Size and Grading on the Shearing Behaviour of Granular Materials, Proc. 6th Int. Conf. Soil. Mech. and Foundation Engineering, Canada, Vol. I, 1965.

[9] R.J. Marsal, Mechanical properties of rockfill, Embankemnt-Dam Engineering, R.C. Hirschfeld and S. J. Poulos, Eds. A Wiley Interscience Publication, 1973.

[10] N.D. Marschi, C.K. Chan, H.B. Seed, Evaluation of Properties of Rockfill Materials, Journal of the Soil Mechanics and Foundations Division, 98(1) (1972) 95-114.

[11] S. Zelasko, R.J. Krizek, T.B. Edil, Shear behavior of sand as a function of grain characteristics, Proc. Conference on Soil Mechanics and Foundation Engineering, Istanbul, 1975.

[12] P. Vangla, G.M. Latha, Influence of Particle Size on the Friction and Interfacial Shear Strength of Sands of Similar Morphology, International Journal of Geosynthetics and Ground Engineering, 1(1) (2015) 6.

[13] R.M. Koerner, Effect of Particle Characteristics on Soil Strength, Journal of the Soil Mechanics and Foundations Division, 96(4) (1970) 1221-1234.

[14] G. Shang, L. Sun, S. Li, X. Liu, W. Chen, Experimental study of the shear strength of carbonate gravel, Bulletin of Engineering Geology and the Environment, 79(5) (2020) 2381-2394.

[15] R. Alias, A. Kasa, M.R. Taha, Particle size effect on shear strength of granular materials in direct shear test, International Journal of Civil and Environmental Engineering, 8(11) (2014) 1144-1147.

[16] X. Zhang, P. Tahmasebi, Effects of Grain Size on Deformation in Porous Media, Transport in Porous Media, 129(1) (2019) 321-341.

[17] A. Boudia, A. Berga, Effect of Grain Size and Distribution on Mechanical Behavior of Dune Sand, Civil Engineering Journal, 7(8) (2021) 1355-1377.

[18] G.-C. Cho, J. Dodds, J.C. Santamarina, Particle Shape Effects on Packing Density, Stiffness, and Strength: Natural and Crushed Sands, Journal of Geotechnical and Geoenvironmental Engineering, 132(5) (2006) 591-602.

[19] C.A. Bareither, T.B. Edil, C.H. Benson, D.M. Mickelson, Geological and Physical Factors Affecting the Friction Angle of Compacted Sands, Journal of Geotechnical and Geoenvironmental Engineering, 134(10) (2008) 1476-1489.

[20] J.S. Zelasko, An investigation of the influences of particle size, size gradation and particle shape of the shear strength and packing behavior of quartziferous sands, Ph.D. thesis, Northwestern Univ., Evanston, Ill, 1966.

[21] T.B. Edil, R.J. Krizek, J.S. Zelasko, Effect of grain characteristics on packing of sands, , in: Proceedings of Istanbul Conf. on Soil Mechanics and Foundation Engineering, Balkema, Rotterdam, 1975, pp.46– 54.

[22] C.H. Juang, P.C. Lu, Predicting Geotechnical Parameters of Sands from CPT Measurements Using Neural Networks, Computer-Aided Civil and Infrastructure Engineering, 17 (2002) 31–42.

[23] G.W. Ellis, C. Yao, R. Zhao, D. Penumadu, Stress-Strain Modeling of Sands Using Artificial Neural Networks, Journal of Geotechnical Engineering, 121(5) (1995) 429-435.

[24] J. Ghaboussi, D.E. Sidarta, New nested adaptive neural networks (NANN) for constitutive modeling, Computers and Geotechnics, 22(1) (1998) 29-52.

[25] J.-H. Zhu, M.M. Zaman, S.A. Anderson, Modeling of soil behavior with a recurrent neural network, Canadian Geotechnical JournaL, 35(5) (1998) 858-872.

[26] W.C. Krumbein, Measurement and geological significance of shape and roundness of sedimentary particles, Journal of Sedimentary Research, 11(2) (1941) 64-72.

[27] ASTM D2487-11, Standard Practice for Classification of Soils for Engineering Purposes (Unified Soil Classification System), ASTM International, West Conshohocken, PA, 2011.

[28] ASTM D4253-16, Standard Test Methods for Maximum Index Density and Unit Weight of Soils Using a Vibratory Table, ASTM International, West Conshohocken, PA, 2016.

[29] ASTM D4254-16, Standard Test Methods for Minimum Index Density and Unit Weight of Soils and Calculation of Relative Density, ASTM International, West Conshohocken, PA, 2016.

[30] ASTM D3080 / D3080M-11, Standard Test Method for Direct Shear Test of Soils under Consolidated Drained Conditions, ASTM International, West Conshohocken, PA, 2011.

[31] M. Riedmiller, H. Braun, A direct adaptive method for faster backpropagation learning: the RPROP algorithm, in: IEEE International Conference on Neural Networks, 1993, pp. 586-591 vol.581.

[32] M.T. Hagan, M. Menhaj, Training feedforward networks with the Marquardt algorithm, IEEE Transactions on Neural Networks, 5(6) (1994) 989–993.

[33] D.J.C. MacKay, A Practical Bayesian Framework for Backpropagation Networks, Neural Computation, 4(3) (1992) 448-472.

[34] F.D. Foresee, M.T. Hagan, Gauss-Newton approximation to Bayesian learning, in: Proceedings of International Conference on Neural Networks (ICNN'97), 1997, pp. 1930-1935 vol.1933.

[35] M.F. Moller, A scaled conjugate gradient algorithm for fast supervised learning, Neural Networks, 6(4) (1993) 525-533.

[36] W. Gander, M.J. Gander, Scientific Computing - An Introduction using Maple and MATLAB, Texts in Computational Science and Engineering, 2014.

[37] G.A.F. Seber, C.J. Wild, Nonlinear regression, Hoboken, NJ: Wiley-Interscience, 2003.

HOW TO CITE THIS ARTICLE

M. Mousavi, M. Jiryaei Sharahi, Estimating the Sand Shear Strength from Its Grain Characteristics Using an Artificial Neural Network Model and Multiple Regression Analysis , AUT J. Civil Eng., 5(3) (2021) 403-420.

DOI: 10.22060/ajce.2021.19213.5721